SPECIAL

Global Precipitation Measurement (GPM)

COLLECTION

Comparison of Raindrop Size Distribution between NASA's S-Band Polarimetric Radar and Two-Dimensional Video Disdrometers

ALI TOKAY,[a,b] LEO PIO D'ADDERIO,[c] DAVID A. MARKS,[d,e] JASON L. PIPPITT,[d,b] DAVID B. WOLFF,[e] AND WALTER A. PETERSEN[f]

[a] *Joint Center for Earth Systems Technology, University of Maryland, Baltimore County, Baltimore, Maryland*
[b] *NASA Goddard Space Flight Center, Greenbelt, Maryland*
[c] *Department of Physics and Earth Science, University of Ferrara, Ferrara, Italy*
[d] *Science System Applications Inc., Lanham, Maryland*
[e] *NASA Goddard Space Flight Center, Wallops Flight Facility, Wallops Island, Virginia*
[f] *NASA Marshall Space Flight Center, Huntsville, Alabama*

ABSTRACT

The ground-based-radar-derived raindrop size distribution (DSD) parameters—mass-weighted drop diameter D_{mass} and normalized intercept parameter N_W—are the sole resource for direct validation of the National Aeronautics and Space Administration (NASA) Global Precipitation Measurement (GPM) mission *Core Observatory* satellite-based retrieved DSD. Both D_{mass} and N_W are obtained from radar-measured reflectivity Z_H and differential reflectivity Z_{DR} through empirical relationships. This study uses existing relationships that were determined for the GPM ground validation (GV) program and directly compares the NASA S-band polarimetric radar (NPOL) observables of Z_H and Z_{DR} and derived D_{mass} and N_W with those calculated by two-dimensional video disdrometer (2DVD). The joint NPOL and 2DVD datasets were acquired during three GPM GV field campaigns conducted in eastern Iowa, southern Appalachia, and western Washington State. The comparative study quantifies the level of agreement for Z_H, Z_{DR}, D_{mass}, and $\log(N_W)$ at an optimum distance (15–40 km) from the radar as well as at distances greater than 60 km from radar and over mountainous terrain. Interestingly, roughly 10%–15% of the NPOL Z_H–Z_{DR} pairs were well outside the envelope of 2DVD-estimated Z_H–Z_{DR} pairs. The exclusion of these pairs improved the comparisons noticeably.

1. Introduction

Estimation of the mass-weighted mean drop diameter D_{mass} to within ±0.5-mm accuracy from the Dual-Frequency Precipitation Radar (DPR) on board National Aeronautics and Space Administration (NASA) Global Precipitation Measurement (GPM) *Core Observatory* is one of the level 1 science requirements of the GPM mission (Skofronick-Jackson et al. 2017). The GPM DPR algorithm adopted a normalized gamma raindrop size distribution (DSD) defined by D_{mass}, the normalized intercept parameter N_W, and the shape parameter μ (Seto et al. 2013). The shape parameter is assumed to be constant with $\mu = 2$ for the combined radar–radiometer algorithm (Grecu et al. 2016) and $\mu = 3$ for the DPR algorithm (Iguchi et al. 2017). The accuracy of the DPR-derived

D_{mass} and N_W is evaluated through direct comparison of ground-based radar products following volumetric footprint matching.

The GPM ground validation team routinely processes a select subset of 70+ National Weather Service (NWS) dual-polarization radars as well as several research radars over the United States with an addition of several tropical and high-latitude oceanic sites for all GPM core satellite overpasses (Pippitt et al. 2015). This labor-intensive, quality-controlled dataset includes D_{mass} and N_W and is produced using the Validation Network architecture (Schwaller and Morris 2011). The D_{mass} and N_W are derived from dual-polarized radar measurements of horizontal reflectivity Z_H and differential reflectivity Z_{DR} through empirical $D_{\mathrm{mass}}(Z_{\mathrm{DR}})$ and $N_W(Z_H, D_{\mathrm{mass}})$ relationships. In turn, the empirical relationships are based on combined analysis of two-dimensional video disdrometer (2DVD) data obtained

Corresponding author: Ali Tokay, tokay@umbc.edu

during six different GPM field campaigns (Tokay et al. 2020).

From the perspective of ground validation traceability, it is important to evaluate the accuracy of the ground-based-radar-derived DSD. Historically, the radar-derived products are often evaluated through comparative studies with surface measurements, which are considered as a reference. For the radar rainfall estimate, there are numerous studies in the literature on quantitative analysis of radar-estimated and gauge-measured rainfall (Cifelli et al. 2011; Giangrande et al. 2014a). For radar-derived DSD, however, there are a limited number of studies where radar-estimated and disdrometer-measured DSD parameters have been compared (Brandes et al. 2004, hereinafter B04; Thurai et al. 2012, hereinafter T12). This is mainly due to the unavailability of such datasets; however, they have recently become more plentiful through NASA GPM and the U.S. Department of Energy Atmospheric Radiation Measurement Program's (Giangrande et al. 2014b) field studies.

Both B04 and T12 were event-based studies in which a single 2DVD was 38 and 15 km from S- and C-band polarimetric radars, respectively. Both studies derived empirical relationships between radar observables of Z_H and Z_{DR} and constrained gamma DSD parameters of median volume diameter D_0 and N_W using simulated and disdrometer-based size distributions and prescribed drop shapes. Comparative studies are subject to measurement errors from both radars and disdrometers, as well as the time–height ambiguity and significant sampling volume differences. Measurement errors can be mitigated by calibrating radar and disdrometer while the time–height ambiguity depends on the characteristics of precipitation and the experimental setup. Both B04 and T12 selected relatively uniform stratiform events where the radar pixel was approximately 350 and 250 m above ground, respectively. B04 and T12 showed good agreement between radar-derived and disdrometer-calculated D_0 and $\log(N_W)$. A key to their success in estimating D_0 and $\log(N_W)$ was the good agreement between radar-measured and disdrometer-calculated Z_H and Z_{DR}.

One of the main causes of the discrepancy between disdrometer- and radar-measured or disdrometer- and radar-derived parameters is the vertical variability of precipitation. As the distance between the disdrometer and radar measurement increases, the radar pulse volumes and the vertical variability of hydrometeors increases and becomes more complicated in the presence of mixed or frozen particles at the radar pixel height. The radar measurements are also vulnerable to surface clutter. Despite the error sources listed above, there is merit in quantifying the differences between disdrometer

and radar measurements at various disdrometer-radar distances, different climate regimes, and various weather systems. Comparative studies provide a realistic range of differences between the two platforms for measured and derived parameters.

This study is dedicated exclusively to the quantification of observed differences in DSD parameters between radar and disdrometer platforms. The dataset used in this study had several diverse features. The precipitation systems were originated both over the land and over the ocean. Both frontal and orographic lifting initiated the precipitation formation. Airmass thunderstorms and mesoscale convective systems provided abundant precipitation. The rest of the paper is organized as follows: Section 2 summarizes the database used in this study. Section 3 describes the mathematical form of the relationships between the DSD parameters of D_{mass} and N_W and dual-polarization radar observables of Z_H and Z_{DR} with the derivation methods using disdrometer datasets. Section 4 presents a comparative study of the disdrometer-calculated and radar-measured radar parameters of Z_H and Z_{DR} as well as disdrometer-calculated and radar-estimated D_{mass} and N_W. A dedicated section 4c describes the fraction of the radar-based Z_H and Z_{DR} pairs that were outside the envelope of the disdrometer observations. Conclusions are presented in section 5.

2. Database

The database was constructed from coincident NASA's S-band polarimetic radar (NPOL) and 2DVD observations during three GPM ground validation (GV) field campaigns: the Iowa Flood Studies (IFloodS), the Integrated Precipitation and Hydrology Experiment (IPHEx), and the Olympic Mountain Experiment (OLYMPEx). Figure 1 depicts the position of the 2DVDs with respect to the NPOL during these field campaigns, and Table 1 lists the location and duration of the field campaigns as well as the number of 2DVDs and their sampling size.

Considering the NPOL database, Z_{DR} was calibrated by vertical profiles of natural precipitation targets (Gorgucci et al. 1999). Absolute Z_H calibration was then determined via self-consistency of the polarimetric variables (Ryzhkov et al. 2005) and the stability of the calibration was monitored using the relative calibration adjustment (Silberstein et al. 2008; Wolff et al. 2015). After labor-intensive quality control of NPOL data for ground clutter and nonmeteorological echo removal and subsequent calibration (Pippitt et al. 2015), the radar data were ready for analyses. Nine radar pixels, one directly above the 2DVDs and eight neighboring pixels, were identified and extracted for this study. It should be noted that it is not feasible to totally avoid ground clutter, especially when it is embedded
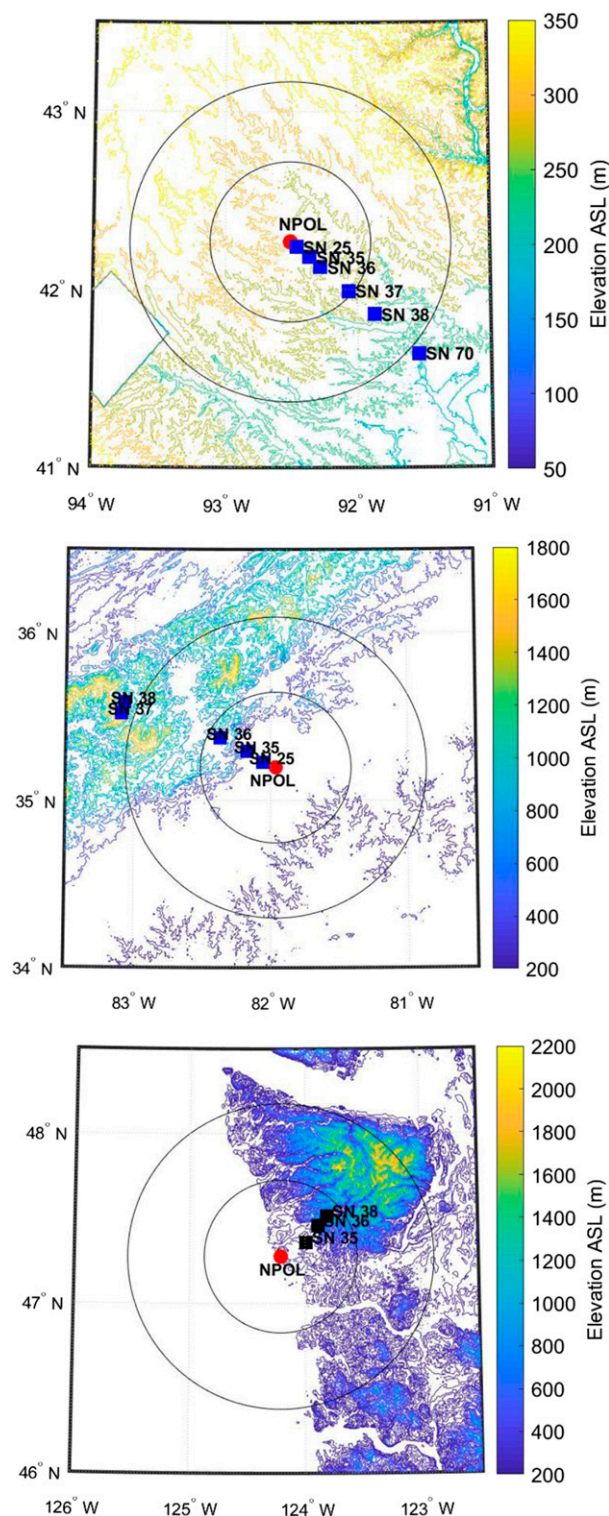
FIG. 1. Position of the 2DVDs with respect to NPOL radar during (a) IFloodS, (b) IPHEx, and (c) OLYMPEx. The 50- and 100-km rings of the NPOL radar are also shown.

with meteorological echo. In these cases, clutter cannot be completely removed because high quality control thresholds would remove too much real echo. In addition, higher radar elevation beams can intersect the bright band, especially at far distances. For this study, the comparison of radar observables of Z_H and Z_{DR} and derived DSD parameters of D_{mass} and $\log(N_W)$ are shown for NPOL gates directly above the 2DVDs. A comparative study using the neighboring eight radar pixels did not significantly alter the findings of this study.

Considering the 2DVD database, a ''rain'' threshold was considered as the occurrence of a minimum of 10 drops and minimum rain rate of $0.01 \, \text{mm h}^{-1}$ in 1-min observations. For this study, the average DSD is calculated for three consecutive rainy minutes centered at the radar scan time. A study using 5-, 7-, and 9-min DSD average did not significantly alter the findings of this study. Very light rain was eliminated from the coincident dataset by setting a Z_H threshold of 5 dB to both the NPOL and 2DVD datasets. The Z_{DR} was also bounded by a maximum of 4 dB to be consistent with the conditions of the derived $D_{mass}(Z_{DR})$ relationship. The initial sample sizes that were given in Table 1 reflect the coincident database after the Z_H and Z_{DR} thresholds were applied. The $D_{mass}(Z_{DR})$ relationship has an additional bound on D_{mass} as being greater than 0.5 mm and less than 4.0 mm. The resultant samples after these additional thresholds on D_{mass} were applied to the comparison of DSD parameters and the resultant sample sizes are shown in Table 1 in parenthesis.

In the presence of abundant rainfall and six 2DVD units, IFloodS provided a richer sample of coincident datasets with respect to the other two experiments. During OLYMPEx, rain was also abundant (Zagrodnik et al. 2018) but the coincident sample size was substantially lower with the availability of only three 2DVD units. Despite the fact that five 2DVD units were available during IPHEx, sample sizes were limited as a result of the fewer rain events than during IFloodS and OLYMPEx.

Cumulative distributions of rain rate (RR), D_{mass}, and $\log(N_W)$ showed the diverse nature of rainfall between the three field campaigns (Fig. 2). Light rain $(RR < 1 \, \text{mm h}^{-1})$ occurred the most during IFloodS, while heavy rain $(RR \geq 10 \, \text{mm h}^{-1})$ was most frequently observed during IPHEx (Fig. 2a). The mean RR was substantially higher during IPHEx, while median and maximum RR were distinctly lower during IFloodS and OLYMPEx, respectively (Table 2). These statistics were based on the 3-min-average 2DVD RR that coincides with the radar scan time. The datasets were diverse in terms of population of small $(D < 1 \, \text{mm})$,

TABLE 1. List of the field campaigns, their coordinates as based on the NPOL site, the duration of database, and the number of 2DVD sites and matched sample size between 2DVD and NPOL. The sample size after adopting a $0.5 \leq D_{\mathrm{mass}} \leq 4.0$ mm interval is also given in parentheses.

Field campaign	Coordinates	Duration	2DVD	
			No. of instruments	Sample size
Iowa Flood Studies (IFloodS)—Iowa City and Waterloo, IA	42.27°N, 92.51°W	May–Jun 2013	6	7736 (7078)
Integrated Precipitation and Hydrology Experiment (IPHEx)—Ashville, NC	35.20°N, 81.96°W	May–Jun 2014	5	1345 (1181)
Olympic Mountain Experiment (OLYMPEx)—Olympic Peninsula, WA	47.28°N, 124.21°W	Nov 2015–Jan 2016	3	1634 (1400)

midsize ($1 \leq D < 3$ mm), and large ($D \geq 3$ mm) drops. The OLYMPEx dataset consists of mostly small–midsize raindrops resulting in the highest occurrence of $D_{\mathrm{mass}} <$ 1.2 mm and $\log(N_W) \geq 3.5$ (Figs. 2b,c). For the purpose of this study, we considered D_{mass} of 1.2 mm as a characteristic size such that the DSD samples dominated by small drops have $D_{\mathrm{mass}} < 1.2$ mm. Similarly, $\log(N_W)$ of 3.5 is the characteristic value above which represents the samples with abundant number of raindrops. Both D_{mass} and $\log(N_W)$ characteristic values are subjective and are determined through examining the cumulative distributions of these parameters from six different field studies (Tokay et al. 2020). IPHEx had substantially more samples at $1.2 \leq D_{\mathrm{mass}} < 2.1$ mm range and IFloodS had the highest number of samples at $\log(N_W) < 3.5$ among the three field campaigns. The lowest mean and median D_{mass} and the highest mean and median $\log(N_W)$ were also observed during OLYMPEx. The similarities in the distribution of rain rate and diversities in the distribution of DSD parameters between the IFloodS and OLYMPEx demonstrate the common observation that the similar rain rates can result from completely different contributions of small, medium, and large drops. This was emphasized when rainfall from convective and stratiform clouds was examined in tropical systems (Tokay and Short 1996; Thompson et al. 2015).

3. Method

Bias and absolute bias between NPOL and 2DVD parameters are considered as the two statistics to quantify the results for the comparative study. Bias is the difference between estimated variable X and reference variable Y and therefore is also referred to as relative error. In this study, the 2DVD was considered as the reference instrument and the parameters of interest are Z_H, Z_{DR}, D_{mass}, and $\log(N_W)$. Bias is defined as

$$\mathrm{bias} = \frac{1}{N}\sum_{i=1}^{N}(X_i - Y_i). \qquad (1)$$

Absolute bias (often referred to as mean absolute error) is the absolute value of the difference between the estimated and reference variables:

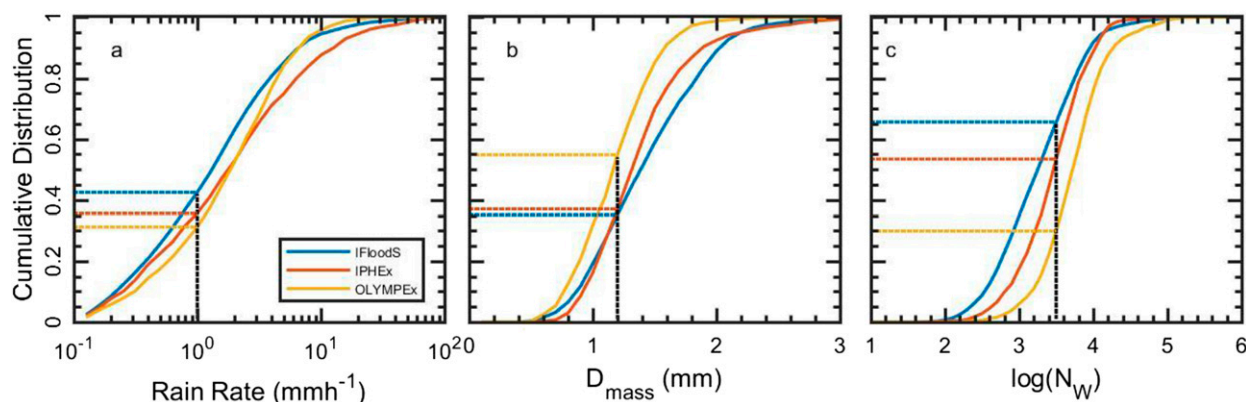$$\mathrm{absolute\ bias} = \frac{1}{N}\sum_{i=1}^{N}|X_i - Y_i|. \qquad (2)$$

FIG. 2. Cumulative distributions of (a) rain rate, (b) mass-weighted drop diameter, and (c) logarithmic normalized intercept parameter of three different 2DVD datasets.

TABLE 2. Mean, median, and maximum of rain rate R, mass-weighted drop diameter D_{mass}, and logarithmic normalized intercept parameter $\log(N_W)$ for three different 2DVD datasets that were used in this study.

2DVD field campaign	R (mm h^{-1})			D_{mass} (mm)			$\log(N_W)$		
	Mean	Median	Max	Mean	Median	Max	Mean	Median	Max
IFoodS	3.06	1.18	143.7	1.40	1.35	4.27	3.64	3.22	5.46
IPHEx	5.01	1.54	152.6	1.35	1.28	3.46	3.64	3.44	4.81
OLYMPEx	2.75	1.71	27.1	1.16	1.15	2.70	3.98	3.70	5.30

Between the two statistics, absolute bias is more reliable for evaluating the level of agreement between the two variables. Considering paired samples on both sides of the 1:1 line, bias could be near zero but absolute bias would be significant if the samples are not near the 1:1 line.

Reflectivities Z_H and Z_{DR} were measured by NPOL and were calculated from size and fall velocity measurements of the 2DVD. Although 2DVD was also capable of measuring drop axis ratios, this study used the laboratory-based observed axis ratios following Andsager et al. (1999) for drops up to 6 mm and equilibrium drop shapes (Beard and Chuang 1987) for drops larger than 6 mm; Z_H and Z_{DR} were derived for S-band wavelength (NPOL's operational frequency) following Rayleigh–Gans theory (Tokay et al. 2002). The Z_{DR} is the ratio of reflectivity at horizontal polarization Z_H to reflectivity at vertical polarization Z_V. The reflectivity at horizontal and vertical polarization is expressed as a function of wavelength λ, dielectric constant of water $|K_{\text{water}}|^2$, and shape factors $S_{H,V}$ as follows:

$$Z_{H,V} = \frac{\lambda^4}{\pi^5 |K_{\text{water}}|^2} \int_{D_{\min}}^{D_{\max}} S_{H,V}(D,r) D^6 N(D)\, dD, \quad (3)$$

where the shape factors are a function of drop axis ratio r. Drop diameter D_{mass} is the ratio of the fourth moment to the third moment of size distribution and is expressed in millimeters. It is calculated from 2DVD size and fall velocity measurements as

$$D_{\text{mass}} = \frac{\int_{D_{\min}}^{D_{\max}} D^4 N(D)\, dD}{\int_{D_{\min}}^{D_{\max}} D^3 N(D)\, dD}. \quad (4)$$

The D_{mass} is also calculated from NPOL Z_{DR} measurements through a third-order polynominal as

$$D_{\text{mass}} = aZ_{DR}^3 + bZ_{DR}^2 + cZ_{DR} + d, \quad (5)$$

where Z_{DR} is in decibels and the a, b, c, and d coefficients are derived from 2DVD datasets for each field campaign (Table 3). Since the 2DVD datasets in each field campaign may not have sufficient sample size at

high Z_{DR} intervals, a generic $D_{\text{mass}}(Z_{DR})$ relationship was derived combining all available 2DVD datasets from six different field campaigns to determine D_{mass} at these ranges. The three additional 2DVD datasets that are not used in this study were collected during the Midlatitude Continental Convective Clouds Experiment in northern Oklahoma, and long-term (more than a year) field studies at the NASA Goddard Space Flight Center Wallops Flight Facility in Wallops Island, Virginia, and the NASA Marshall Space Flight Center in Huntsville, Alabama (Tokay et al. 2020).

Parameter N_W is the normalized intercept parameter and is expressed as a function of D_{mass} in millimeters and liquid water content W in grams per meter cubed, both of which are calculated from 2DVD size and fall velocity measurements. The formulation includes density of water ρ_w in grams per centimeter cubed and several constants that are related to the complete gamma function solution of D_{mass} and W (Testud et al. 2001):

$$N_W = \frac{4^4 10^3 W}{\pi \rho_w D_{\text{mass}}^4}; \quad (6)$$

N_W is analogous to the intercept parameter of the gamma size distribution (Ulbrich 1983) and is therefore sensitive to the number of drops. It has a wide numerical range covering over four orders of magnitude and is therefore expressed in logarithmic units $\log(N_W)$ rather than its linear dimension (m^{-3} mm^{-1}).

Parameter N_W is also retrieved from measured NPOL Z_H and Z_{DR} after D_{mass} is calculated from Eq. (5). The empirical equation is derived combining 2DVD

TABLE 3. The coefficients of the D_{mass}–Z_{DR} relationship and the maximum Z_{DR} range for the three different 2DVD datasets and the combined dataset, which includes three additional field campaigns.

Field campaign	a	b	c	d	max Z_{DR} (dB)
IFloodS	0.1988	−1.0747	2.3786	0.3623	3.05
IPHEx	0.1887	−1.0024	2.3153	0.3834	2.85
OLYMPEx	0.2209	−1.1577	2.3162	0.3486	2.65
ALL	0.0138	−0.1696	1.1592	0.7215	3.95

database from six different field campaigns (Tokay et al. 2020) and is given as

$$N_W = aZ_H D_{\text{mass}}^b, \tag{7}$$

where D_{mass} is in millimeters, Z_H is in linear units ($\text{mm}^6\,\text{m}^{-3}$), and a and b are 35.3 and -7.2, respectively. The coefficient a and exponent b were indistinguishable among the six different field campaigns. Reflectivity Z_{DR} is sensitive to the drop shape, which is spherical for the drops of less than 1 mm (Tokay and Beard 1996). The radar measurements of Z_{DR} are noisy in the presence of abundant small drops and absence of large drops. Using the formulation in Eqs. (5) and (7), when Z_{DR} is 0.1 dB, D_{mass} can still be 0.5 mm or higher but $\log(N_W)$ is greater than 6 at 30 dBZ. The 2DVD observations show that this is an unrealistic DSD (Table 2). The uncertainty in estimating $\log(N_W)$ was mitigated by setting realistic $\log(N_W)$ thresholds between 0.5 and 6.

4. NPOL–2DVD comparisons

The level of agreement between NPOL-measured and 2DVD-calculated Z_H and Z_{DR} is related to the agreement between NPOL-derived and 2DVD-calculated D_{mass} and N_W. Midsize to large drops are the main contributors to the Z_H (Adirosi et al. 2015) and because of its power-weighted nature, Z_{DR} is very sensitive to the presence of a few large drops that have the lowest axis ratios (Tokay et al. 2020). The presence or absence of a few large drops could therefore result in noticeably different 2DVD-calculated Z_H and Z_{DR} values. Both parameters are therefore heavily affected by the differences in sampling volumes of NPOL and 2DVD.

The sampling volume of NWS operational radars can exceed that of the 2DVD by a factor of 10^7 or more at a distance of 30 km (Cao et al. 2008). The disdrometer sampling volume is a multiplicative function of sampling cross section, fall velocity that corresponds to the characteristic size, and sampling interval (Campos and Zawadzki 2000). The cross section of the 2DVD is nominally 0.01 m², and the integration period was 180 s in this study. If mean or median drop size is the characteristic size, the sampling size is less than 15 m³ among the three field campaigns. If maximum drop size is the characteristic size, the sampling volume is less than 18 m³. The sampling volume of the radar depends on the beamwidth, range gate size, and the distance from radar. The beamwidth of NPOL was 0.98° in all three field campaigns, and the range gate was 150 m during IFloodS and 125 m during IPHEx and OLYMPEx. Table 4 lists the 2DVD-NPOL distances as well as NPOL elevation angles and beam heights. For IFloodS, the NPOL sampling volume is 3 378 908 m³

TABLE 4. NPOL elevation angle based on first (label 1st) or second (label 2nd) elevation, beam height at the 2DVD sites, and NPOL–2DVD distance during IFloodS, IPHEx, and OLYMPEx.

2DVD serial no.	IFloodS			IPHEx			OLYMPEx		
	NPOL elev angle (°)	NPOL beam height (km)	NPOL–2DVD distance (km)	NPOL elev angle (°)	NPOL beam height (km)	NPOL–2DVD distance (km)	NPOL elev angle (°)	NPOL beam height (km)	NPOL–2DVD distance (km)
SN 25	1.4 (2nd)	0.123	4.96	1.5 (2nd)	0.244	9.15	—	—	—
SN 35	1.4 (2nd)	0.385	15.20	1.5 (2nd)	0.597	21.73	1.5 (2nd)	0.514	18.85
SN 36	1.4 (2nd)	0.634	24.51	1.5 (2nd)	1.199	41.88	1.5 (2nd)	0.886	31.59
SN 37	1.4 (2nd)	1.290	47.40	1.5 (2nd)	3.549	108.94	—	—	—
SN 38	1.4 (2nd)	1.976	69.31	1.5 (2nd)	3.582	109.78	0.5 (1st)	0.443	39.97
SN 70	0.7 (1st)	1.959	106.14	—	—	—	—	—	—

TABLE 5. Comparison of 2DVD-calculated and NPOL-measured Z_H (dBZ) during IFloodS, IPHEx, and OLYMPEx. Considering Z_H of 2DVD as a reference, bias and absolute bias are presented at each 2DVD site for each field campaign. The sample sizes are also given.

IFloodS			IPHEx			OLYMPEx		
Bias	Absolute bias	Sample size	Bias	Absolute bias	Sample size	Bias	Absolute bias	Sample size
0.50	3.32	1378	1.24	3.60	244	—	—	—
−0.97	3.28	1901	−0.83	5.45	126	1.30	3.70	528
−1.12	3.95	1206	−1.41	4.60	347	1.10	4.39	489
−1.48	4.55	1444	−2.73	6.80	388	—	—	—
−0.61	4.66	855	−2.33	7.10	240	0.52	3.96	617
−0.10	4.57	952	—	—	—	—	—	—

at its closest distance of 5 km and 1 550 794 368 m³ at its farthest distance of 106 km. The NPOL sampling volumes were within this range for the other two field campaigns. The differences in sampling volume ranged from 10^5 to 10^7 orders of magnitude at distances from 5 to 106 km from the radar. The beam heights were calculated on the basis of a 4/3 Earth radius model under standard atmospheric conditions. The possible pitfalls of this model were presented by Zeng et al. (2014) and are beyond the scope of this study. For the sites that are located at higher elevations than the NPOL, the distance of the beam height to the ground is less than what was reported in Table 4. During IPHEX, the farthest three sites (SN36, SN37, and SN38) were 380, 732, and 1072 m higher elevation than the NPOL.

The time–height ambiguity is another source of disagreement between disdrometer and radar measurements. The vertical variability of the DSD results in a nonuniform profile of Z_H and Z_{DR} between the altitude of the radar scan and the ground. For fast moving storms, there is a time lag between the radar scan time and disdrometer observations especially at far distances. These factors are best investigated through collocated vertically pointing radars and disdrometers (Tokay et al. 2009).

Because NPOL is a transportable facility and not situated on a tower (the antenna feed horn is ~8 m above

ground level at an elevation angle of 0°), the first elevation angle is often subject to ground clutter. The second elevation is therefore selected to compare 2DVD and NPOL variables except at the farthest distances during IFloodS and OLYMPEx. It should also be added that no corrections for height-dependent drop fall-speed time lags or vertical wind shear/direction impacts on drop trajectories were applied. Based on the environmental conditions, the bright band was not a factor for this study.

a. Z_H and Z_{DR}

Good agreement was evident between 2DVD-calculated and NPOL-measured Z_H. During IFloodS, the NPOL bias relative to the 2DVD observations ranged from as high as −1.48 dB to +0.50 dB (Table 5). Note that the negative bias shows the underestimation of the NPOL variable while the overestimation of the NPOL variable is depicted with a positive bias. The absolute bias increased with range, spanning values from 3.28 dB at 15 km to 4.66 dB at 69 km range, but was lower at the farthest distance where the vertical distance between the NPOL pixel and 2DVD was less than the closer sites because of the use of first elevation angle (Table 4). While there was large scatter around the 1:1 line (Fig. 3a), the majority of the observations were aligned along the
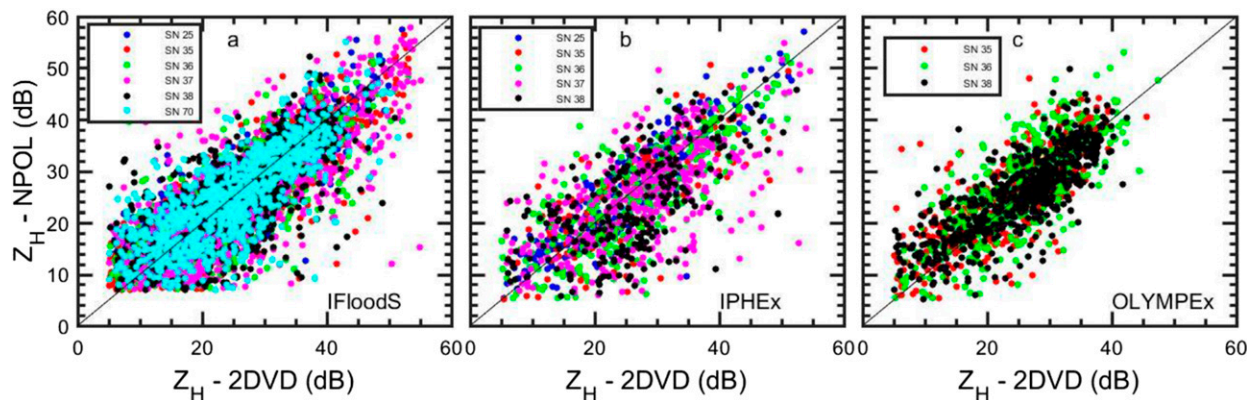

FIG. 3. Scatter diagram of 2DVD-calculated and NPOL-measured Z_H during (a) IFloodS, (b) IPHEx, and (c) OLYMPEx. The colors represent the specific 2DVD site during each field campaign.
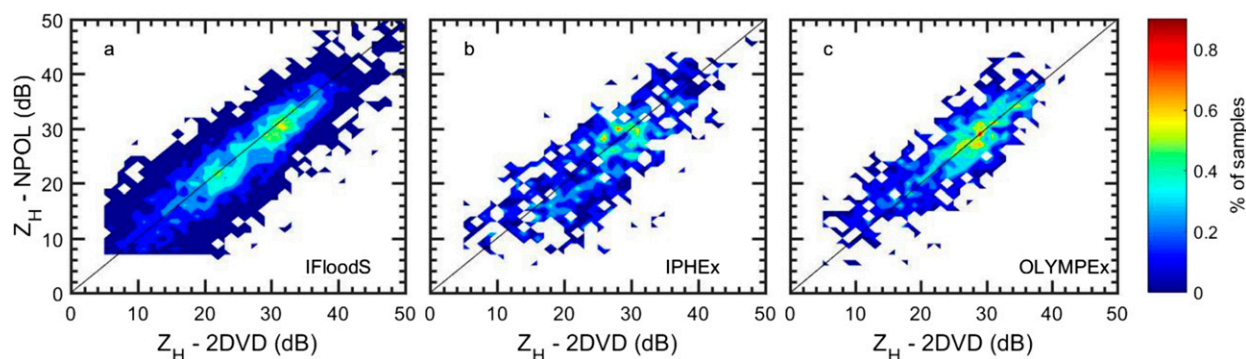
FIG. 4. A 2D density plot of 2DVD-calculated and NPOL-measured Z_H during (a) IFloodS, (b) IPHEx, and (c) OLYMPEx.

1:1 line (Fig. 4a). Several outliers are visible in the figures. Among those, a couple of outliers at the SN37 site had Z_H of 2DVD that was higher than 50 dB and Z_H of NPOL that was less than 20 dB (Fig. 3a).

During IPHEx, the NPOL underestimated Z_H with noticeably high biases of −2.73 and −2.33 dB at the two farthest sites (SN37 and SN38) at ranges greater than 100 km and in higher terrain. The corresponding absolute biases in these two sites, 6.80 and 7.10 dB, were the highest among three field campaigns. A relatively small sample of high Z_H in the 2DVD resulted in this high bias and they were not event specific (Fig. 3b). Among those, one sample at SN37 had Z_H of 2DVD that was higher than 50 dB and Z_H of NPOL that was less than 20 dB. These samples were not visible in the frequency diagram where most of the observations lay on the 1:1 line (Fig. 4b). This demonstrates the importance of both scatter and 2D density diagrams.

During OLYMPEx, the NPOL overestimated Z_H for all three sites but the bias at the farthest site (SN38) was at least one-half of its value of the closest two sites (SN35 and SN36) (Table 5). The absolute bias increased from 3.70 to 4.39 dB between the closest two distances but was 3.96 dB at the farthest distance. The NPOL beam height was 145 m lower at the SN38 site than at the SN35 site because of the differences in elevation angles (Table 4). The SN38 site was also only 8.4 km farther

from NPOL than the SN36 site. Important was that the majority of the observations were aligned with the 1:1 line (Fig. 4c) and the scatter about the 1:1 line was considerably less pronounced, with relatively fewer outliers than the other two field campaigns. Two of the outliers at the SN35 site had Z_H of 2DVD that was less than 10 dB and Z_H of NPOL that was around 35 dB (Fig. 3c).

There were considerable differences between 2DVD-calculated and NPOL-measured Z_{DR}. The Z_{DR} biases were positive, indicating an overestimation by NPOL relative to the 2DVD, at all sites during all three field campaigns, but were drastically different in magnitude between the sites (Table 6). The Z_{DR} bias at its closest 2DVD-NPOL distance was the highest, 0.6 dB, among all sites during IFloodS. The rest of the five sites had low Z_{DR} bias ($< \pm 0.1$ dB). The high bias at the closest site was attributed to surface clutter, which also played a role at the closest 2DVD-NPOL distance during IPHEx. Both sites were less than 10 km of distance from NPOL in respective field campaigns. High Z_{DR} biases were also present at the two farthest sites, which were located at higher elevation, during IPHEx. High biases were mainly driven by the samples of NPOL Z_{DR} that were greater than 2 dB and 2DVD Z_{DR} that were less than 0.5 dB (Fig. 5). The wide scatter on both side of the 1:1 line, on the other hand, reflected the combination of low

TABLE 6. Comparison of 2DVD-calculated and NPOL-measured Z_{DR} (dB) during IFloodS, IPHEx, and OLYMPEx. Considering Z_{DR} of 2DVD as a reference, bias and absolute bias are presented at each 2DVD site for each field campaign.

2DVD serial no.	IFloods		IPHEx		OLYMPEx	
	Bias	Absolute bias	Bias	Absolute bias	Bias	Absolute bias
SN 25	0.60	0.74	0.12	0.36	—	—
SN 35	0.02	0.27	0.00	0.34	0.05	0.32
SN 36	0.02	0.31	0.02	0.30	0.27	0.51
SN 37	0.07	0.34	0.46	0.71	—	—
SN 38	0.07	0.32	0.37	0.66	0.17	0.37
SN 70	0.09	0.35	—	—	—	—
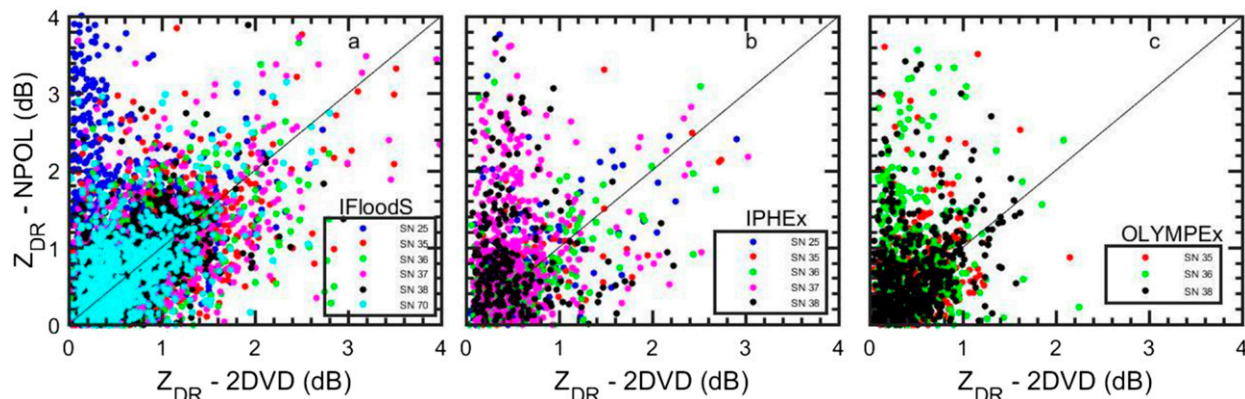
FIG. 5. As in Fig. 3, but for Z_{DR}.

bias (<0.1 dB) and considerably higher absolute bias (0.27–0.35 dB) in Z_{DR} at total of eight sites in three field campaigns (Figs. 5 and 6). This highlights that the low bias itself can mislead for the evaluation of the level of agreement.

b. D_{mass} and N_W

NPOL-based D_{mass} is derived from Z_{DR} and the comparison of D_{mass} between 2DVD and NPOL had similar statistics as for Z_{DR}. The D_{mass} bias was very high—0.32 mm—at the closest NPOL–2DVD distance and was low (≤ 0.05 mm) for the other five sites during IFloodS (Table 7). The D_{mass} biases were also low at all sites except for the two farthest sites (SN37, SN38) where time–height ambiguity was significant during IPHEx. The differences in beam height played a role in determining the D_{mass} bias. During OLYMPEx, D_{mass} bias was very low at SN35 site but the absolute biases in D_{mass} were about the same at SN35 and SN38 sites. Although SN38 site was farthest away from NPOL, the radar beam height was the closest to the ground since the first rather than the second beam was used at SN38 site in this study (Table 4). The absolute bias in D_{mass}

remained less than 0.4 mm at the sites where biases were equal to or less than 0.1 mm during the three field campaigns. The absolute bias in D_{mass} was as high as 0.62 mm at the SN37 site during IPHEx where bias was also the highest—0.34 mm—among the field campaigns. The positive bias in D_{mass} indicates that the mass-weighted size spectrum is shifted toward smaller sizes in 2DVD. This means that the normalized size spectrum will have more small drops and/or a lack of large drops, resulting in lower D_{mass}.

On closer examination, the scatter and 2D density diagrams of 2DVD-calculated and NPOL-estimated D_{mass} revealed wide scatter from 1:1 line especially during IFloodS (Fig. 7). At the same time, a majority of the observations aligned on the 1:1 line during IFloodS, while they diverge from the 1:1 line biased toward NPOL and 2DVD D_{mass} during IPHEx, and OLYMPEx, respectively (Fig. 8). There were no site-specific outliers in each field campaign except a small cluster of outliers were visible at NPOL-estimated D_{mass} that are greater than 3 mm during OLYMPEx (Fig. 7c). The scatter diagram also showed five samples of 2DVD-calculated D_{mass} that were larger than 3.6 mm during
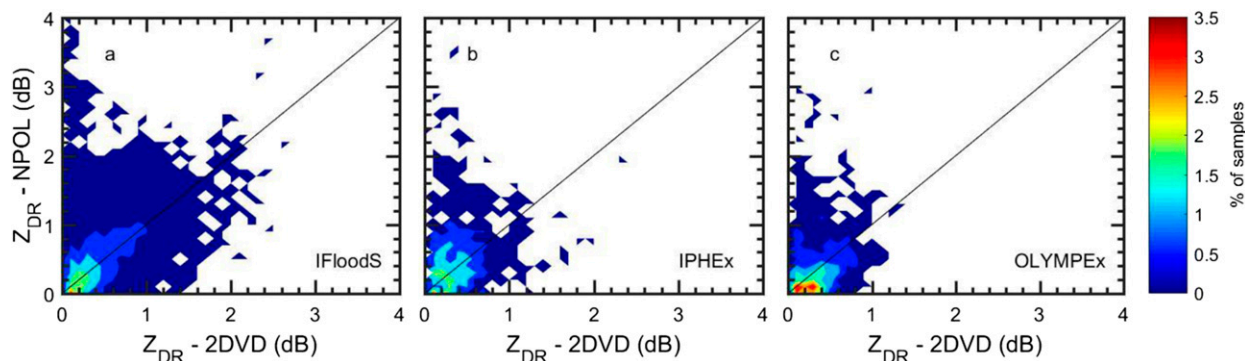

FIG. 6. As in Fig. 4, but for Z_{DR}.

TABLE 7. Comparison of 2DVD-calculated and NPOL-estimated D_{mass} (mm) during IFloodS, IPHEx, and OLYMPEx. Considering D_{mass} of 2DVD as a reference, bias and absolute bias are presented at each 2DVD site for each field campaign. The sample sizes are also given.

2DVD serial no.	IFloods			IPHEx			OLYMPEx		
	Bias	Absolute bias	Sample size	Bias	Absolute bias	Sample size	Bias	Absolute bias	Sample size
SN 25	0.32	0.51	1193	0.03	0.35	217	—	—	—
SN 35	−0.02	0.31	1757	0.04	0.37	116	0.02	0.36	439
SN 36	−0.03	0.34	1124	0.00	0.34	310	0.21	0.46	413
SN 37	0.05	0.33	1324	0.34	0.62	336	—	—	—
SN 38	0.04	0.37	803	0.25	0.58	209	0.11	0.38	552
SN 70	0.04	0.37	877	—	—	—	—	—	—

IFloodS (Fig. 7a). These samples were underestimated by NPOL with no range dependency.

N_W is a function of both Z_H and D_{mass} and the $\log(N_W)$ statistics followed somewhat similar trends as D_{mass}. Absolute biases of $\log(N_W)$ were less than 1 except the nearest 2DVD site (SN25) during IFloodS, the farthest two sites (SN37 and SN38) during IPHEx and the middle site (SN36) during OLYMPEx (Table 8). The $\log(N_W)$ bias was near 0.6 and negative at the nearest site where ground clutter was the factor during IFloodS. The negative and high biases were also present at two farthest sites during IPHEx. The biases were relatively low during OLYMPEx where the highest bias—0.27—was at the closest site (SN35). N_W is related to the peak of the number of drops per given volume per size interval and the drop counts per volume typically decreases with size. The negative bias therefore indicates fewer drops per volume in NPOL and the vice versa is true for positive bias.

The order of magnitude of $\log(N_W)$ was substantially higher and was at the limits of the GPM GV DSD retrieval algorithm for NPOL-derived $\log(N_W)$. The vast majority of the 2DVD observations, on the other hand, were within values $\log(N_W)$ of 2–4.5 (Figs. 9 and 10).

Following Eq. (7), high Z_H and low D_{mass} results in high $\log(N_W)$. The unlikely combination of Z_H of 45 dB and D_{mass} of 1.4 mm, for instance, corresponds to $\log(N_W)$ of 5. The combination of Z_H of 30 dB and D_{mass} of 3.1 mm, on the other hand, results in $\log(N_W)$ of 1. Although these pairs do not exist in the 2DVD database, they exist in the NPOL database since D_{mass} is the derived quantity. It is therefore expected that the estimation of $\log(N_W)$ is poorer than the estimation of D_{mass}.

c. Outliers

The diagram of Z_H/Z_{DR} fields, which have been previously used for determining hail by radar (Aydin et al. 1986), precipitation segments (e.g., stratiform rain vs thunderstorm core), and precipitation type (e.g., continental vs tropical) by disdrometer (Zhang et al. 2006; Kumjian 2013), shows the major differences in radar and disdrometer observations. Cao et al. (2008) who overlaid 2DVD and dual-polarization-radar-based Z_H/Z_{DR} fields, marked the high Z_{DR} region observed by radar only. This region is attributed to the leading edge of convection with large drops and relatively low drop concentrations. As noted by Kumjian (2013), Z_{DR} varies with drop size and shape and a few large drops can result in
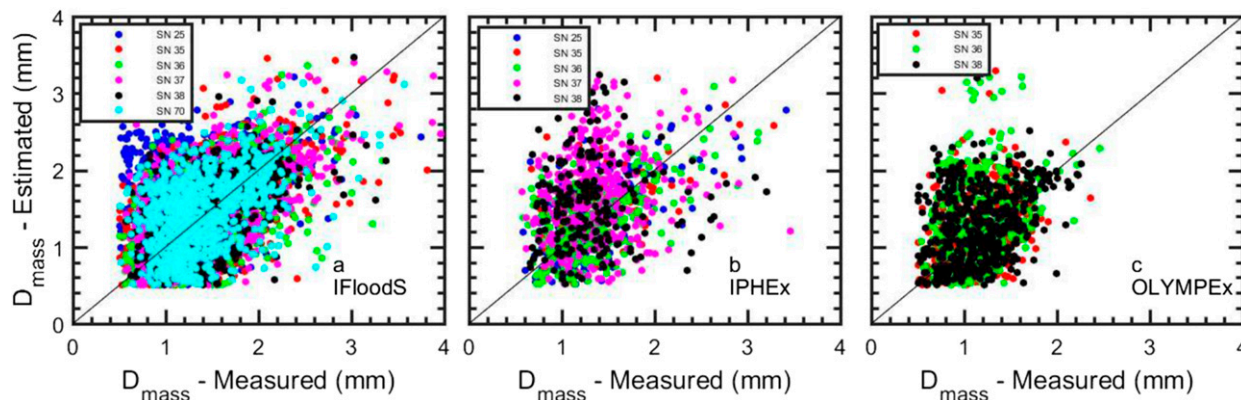

FIG. 7. Scatter diagram of 2DVD-calculated and NPOL-estimated D_{mass} during (a) IFloodS, (b) IPHEx, and (c) OLYMPEx. The colors represent the specific 2DVD site during each field campaign.
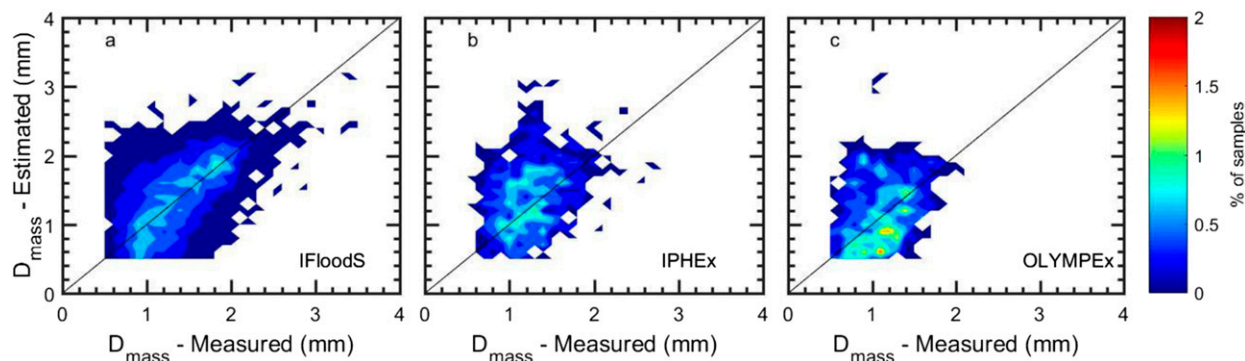
FIG. 8. A 2D density plot of 2DVD-calculated and NPOL-estimated D_{mass} during (a) IFloodS, (b) IPHEx, and (c) OLYMPEx.

very high Z_{DR} values ($>$2.5 dB). Z_H, on the other hand, is directly proportional to the particle concentration and may have moderate values (25–30 dB). Given the fact that the sample volume of the disdrometers is much smaller than the radar, the relatively infrequent big drops may not be caught by the disdrometer.

The 2DVD observations from three field sites were merged to determine the boundaries of the envelope of the Z_H/Z_{DR} field (Fig. 11a). The envelope was wide in both Z_H and Z_{DR} space. At Z_H of 40 dB, Z_{DR} ranged from 0.3 to 3.8 dB. Similarly, at Z_{DR} of 1 dB, Z_H ranged from 15 to 50 dB. The majority of the observations fell in much narrower range centering at Z_H of 20 dB and Z_{DR} of 0.2 dB (Fig. 11b). The NPOL Z_H/Z_{DR} observations outside the 2DVD Z_H/Z_{DR} envelope mostly occurred at moderate-to-high Z_{DR} and low-to-moderate Z_H regime (Regime I) (Fig. 11c). The IPHEx radar data had the highest percentage, 15%, of observations with respect to IFloodS and OLYMPEx in this regime (Table 9). The low Z_{DR} and high Z_H regime (Regime II), on the other hand, had 2% or less of the observations in a given field campaign. None of the two regimes corresponded to a particular segment of the storms. There was no correlation between the leading edge of the convective events and Regime I as previously reported by Cao et al. (2008).

The combined Regimes I and II consist of 15% of the observations during IPHEx, 5% and 5.5% higher than the OLYMPEx and IFloodS, respectively. The recalculated bias and absolute bias after eliminating observations in these two regimes was noticeably less for Z_{DR} and $\log(N_W)$ and marginally less for Z_H and D_{mass} (Table 9). The reduction in absolute bias was 0.35 and 0.12 dB for Z_H and Z_{DR} and 0.05 mm and 0.14 for D_{mass}, and $\log(N_W)$, respectively, during IPHEx.

The majority of the Regime-I samples occurred with Z_H of less than 30 dB, with a slight bias toward the 2DVD observations (Fig. 12a). The Regime-II samples occurred with Z_H of higher than 30 dB, with no significant bias. The observations for Regimes I and II were very distinct in Z_{DR} (Fig. 12b). Almost all of the Regime-I observations occurred in a narrow zone where Z_{DR}-2DVD was less than 0.6 dB and Z_{DR}-NPOL was above 0.2 dB. The Regime-II observations, on the other hand, were mainly observed at Z_{DR}-NPOL less than 0.4 dB and Z_{DR}-2DVD less than 1 dB. Regime I corresponded to the overestimation of D_{mass} and underestimation of $\log(N_W)$ by NPOL, and the vice versa is true for Regime II (Figs. 12c,d). Observations for both Regime I and Regime II fell into the envelope of the rest of the observations in D_{mass} but were at the edge of the observations in $\log(N_W)$. The reduction of dynamic range

TABLE 8. Comparison of 2DVD-calculated and NPOL-estimated $\log(N_W)$ during IFloodS, IPHEx, and OLYMPEx. Considering $\log(N_W)$ of 2DVD as a reference, bias and absolute bias are presented at each 2DVD site for each field campaign.

| 2DVD serial no.	IFloods		IPHEx		OLYMPEx	
	bias	Absolute bias	bias	Absolute bias	bias	Absolute bias
SN 25	−0.59	1.05	0.17	0.90	—	—
SN 35	0.06	0.73	−0.01	0.85	0.27	0.98
SN 36	0.07	0.78	−0.04	0.87	−0.19	1.08
SN 37	−0.15	0.83	−0.81	1.24	—	—
SN 38	0.04	0.72	−0.62	1.22	−0.08	0.94
SN 70	0.00	0.88	—	—	—	—
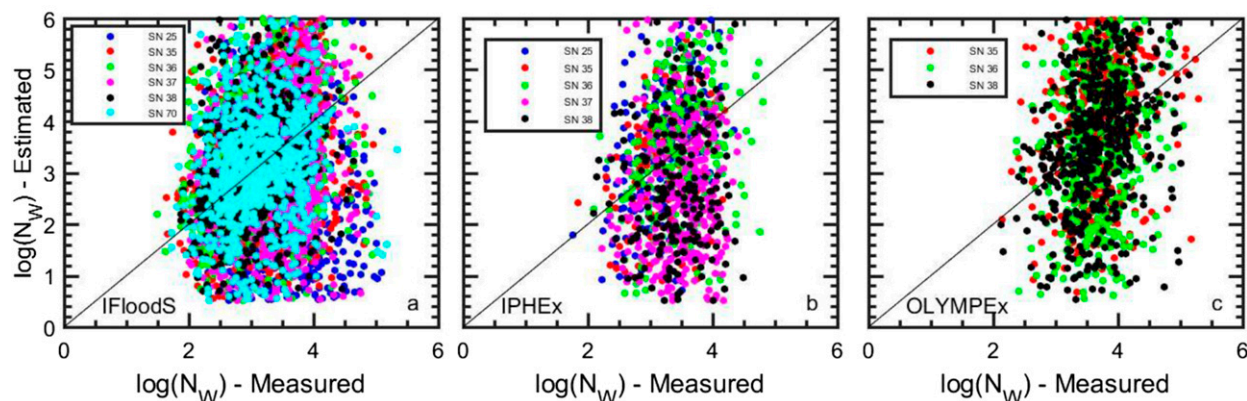
FIG. 9. As in Fig. 7, but for $\log(N_W)$.

of NPOL-estimated $\log(N_W)$ resulting from the absence of Regime I was significant.

A key question relates to the origin of Regimes I and II in NPOL observations. The 2DVD is widely used as a reference instrument for DSD measurements (Tokay et al. 2013). The underestimation of small drops has been recognized and recently investigated through field studies where 2DVD was collocated with a Meteorological Particle Spectrometer (Thurai and Bringi 2018). In this study, we tested three DSDs that had abundant small drops and maximum drop diameter of 2.9 mm or less. These DSDs had Z_{DR} of 0.43–0.55 dB, very similar to Regime-II Z_{DR} values. The corresponding Z_H ranged between 29.1 and 35.7 dB. Considering that 0.9 mm is the smallest drop size where 2DVD has the correct drop number counts, we reassigned drop concentration for the first size bins, 0.1–0.7 mm, extending the slope of the distribution such that the modified DSDs had essentially an exponential distribution. While total concentration drastically increased before and after the modified DSD, the increase in Z_H was less than 0.1 dB. This exercise showed that Regime II was not related to underestimation of small drops by 2DVD. Given the

fact that the radar samples much greater volume than the disdrometer, it is feasible that the disdrometer may not sample less-frequent large drops. We artificially added a single drop at 1-, 2-, and 3-mm diameter larger than the observed D_{max} of the three samples mentioned above. The presence of the additional drop enhanced Z_H and Z_{DR} as much as 6 and 2.3 dB, respectively, but it did not cross over to Regime I or II. It was also evident that NPOL observations in Regimes I and II were present regardless of 2DVD site distance to radar throughout field campaigns. Since this study was based on NPOL measurements, we questioned whether Regimes I and II exist in operational radars. Indeed, Regime I and Regime II do exist in NWS dual-polarization radars. To differentiate these unrealistic DSDs in radar observations, a matrix of Z_H/Z_{DR} was created following Fig. 11c and is shown in Fig. 11d.

5. Conclusions

This study was motivated by the fact that the dual-polarization radar-based N_W and D_{mass} are required products for the validation of GPM DPR N_W and D_{mass} estimates. More specifically, the evaluation of the
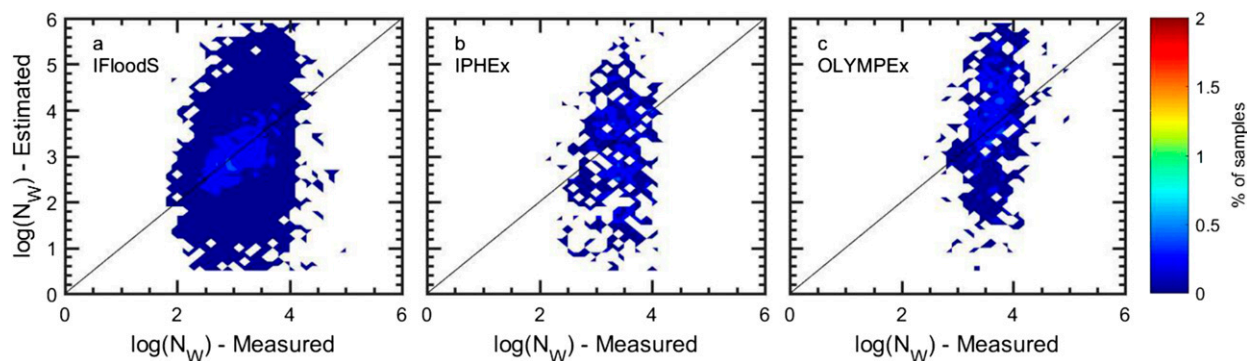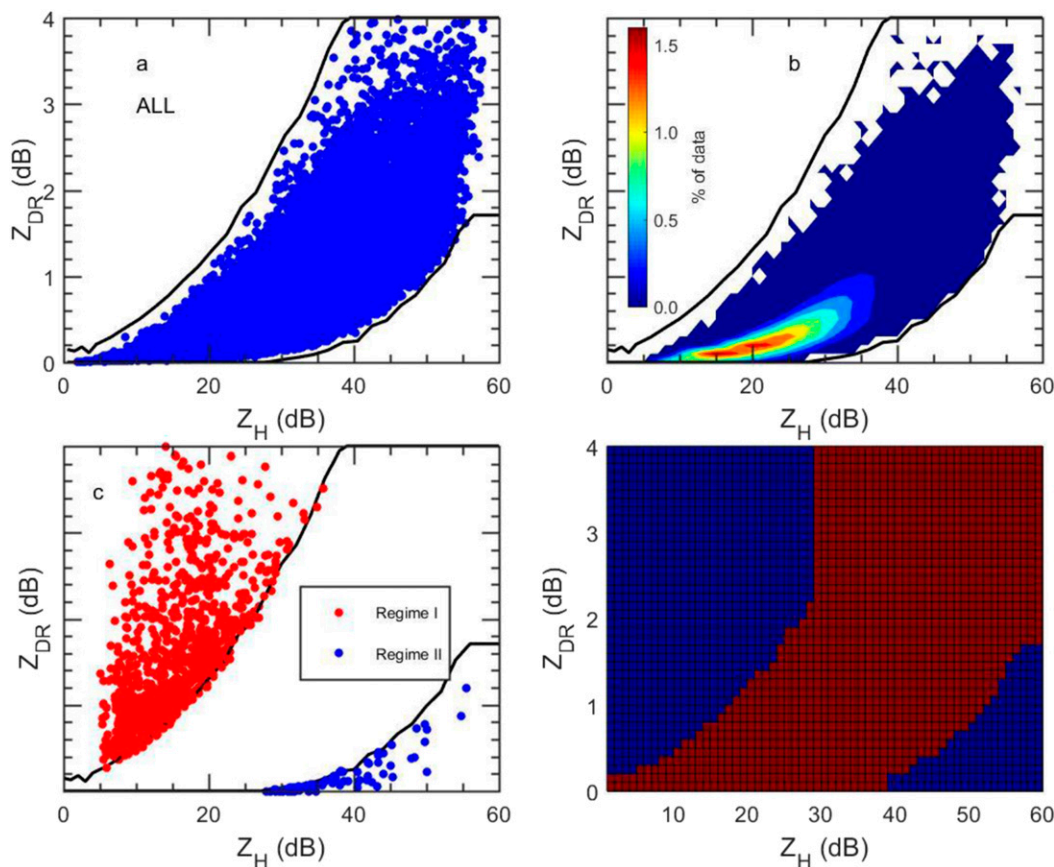

FIG. 10. As in Fig. 8, but for $\log(N_W)$.

FIG. 11. (a) Envelope of 2DVD-calculated Z_H and Z_{DR}. The 2DVD database is from the three field campaigns listed in Table 1. (b) A 2D density plot of 2DVD-calculated Z_H and Z_{DR}. (c) NPOL-measured Z_H and Z_{DR} fields outside the 2DVD Z_H and Z_{DR} envelope. Regimes and I and II denote high Z_{DR}–low Z_H fields and low Z_{DR}–high Z_H fields, respectively. (d) The Z_H/Z_{DR} matrix. The matrix consists of 60 Z_H columns and 40 Z_{DR} rows where Z_H ranged from 0 to 60 dB with 1-dB bin width and Z_{DR} ranged from 0 to 4 dB with 0.1-dB bin width. Regimes I and II are shaded in blue.

ground-radar-based D_{mass} is a requirement for the GPM GV program because it is a NASA level 1 science requirement for the GPM mission. Algorithm developers seek information on possible shortcomings of both ground- and spaceborne radar DSD estimates. A comparative study of radar-measured and disdrometer-calculated Z_H and Z_{DR} is the basis but is also a difficult task for evaluating radar-derived DSD parameters. Previous studies carefully selected and examined the agreement between disdrometer/radar Z_H and Z_{DR} pairs at optimum radar-disdrometer distance (15–40 km at S-band) (B04; T12), which is shorter for higher-frequency radars. This study included one or two *optimum* sites in each field campaign, but the ground clutter was a factor at the lowest elevation angle due to the site of NPOL antenna at the top of the container rather than on a tower. Using the second-lowest elevation, the NPOL beam height was 369 m above the ground at a distance of 15.2 km. This is comparable to the previous

studies as being the best-case scenario. For most of the field studies including radar-estimated and gauge-measured rainfall comparative studies (Giangrande and Ryzhkov 2008; Cunha et al. 2013), the logistics did not allow deployment of the in situ devices near the radar site. Having the 2DVDs at various ranges from the NPOL radar (Fig. 1) enabled this study to quantify the level of agreement with distance.

As the best-case scenario, the absolute biases of Z_H and Z_{DR} were relatively low, ranging from 3.3 to 3.7 and from 0.27 to 0.32 dB, respectively at the shortest distance (15–20 km from the radar) in the absence of surface clutter for the three field campaigns. The corresponding absolute biases of D_{mass} and $\log(N_W)$ were 0.31–0.36 mm and 0.34–0.98, respectively. The absolute bias in Z_H increased with distance but was relatively low at the farthest distance during IFloodS and OLYMPEx where the first elevation rather than the second elevation was used for the comparative study. Specifically, the absolute

TABLE 9. Comparison of 2DVD-calculated and NPOL-measured/estimated Z_H, Z_{DR}, D_{mass}, and $\log(N_W)$ before and after removal of the Z_H–Z_{DR} pairs outside the 2DVD Z_H–Z_{DR} envelope during IFloodS, IPHEx, and OLYMPEx. The bias and absolute bias statistics are given before (italics) and after (boldface) the removal of Regime I and II clusters. The reduction in sample size and its partitioning after removal of Regime I and II are also given.

Field campaigns	Bias	Absolute bias	Bias	Absolute bias	Percent reduction in sample size
			Z_H (dB)		
IFloods	−0.68	3.94	**−0.59**	**3.84**	9.5
IPHEx	−1.41	5.58	**−0.86**	**5.23**	15.0
OLYMPEx	0.95	4.01	**0.94**	**3.89**	10.0
			Z_{DR} (dB)		
IFloods	0.15	0.39	**0.03**	**0.29**	9.5
IPHEx	0.22	0.50	**0.08**	**0.38**	15.0
OLYMPEx	0.16	0.40	**0.07**	**0.31**	10.0
			D_{mass} (mm)		
IFloods	0.06	0.37	0.00	**0.34**	6.6
IPHEx	0.15	0.47	**0.07**	**0.42**	10.4
OLYMPEx	0.11	0.40	**0.03**	**0.34**	8.4
			$\log(N_W)$		
IFloods	−0.10	0.83	**0.04**	**0.74**	6.6
IPHEx	−0.32	1.04	**−0.12**	**0.90**	10.4
OLYMPEx	0.00	0.99	**0.19**	**0.88**	8.4

biases of Z_H were about the same at 47.4 and 106.1 km distances from radar but the difference in the NPOL beam height was only 129 m because of the choice of first versus second elevation angles during IFloodS. This highlights the importance of time–height ambiguity.

During IPHEx, the absolute biases of Z_H were higher at a given distance than during the other two field campaigns. This could be result of higher occurrence of heavy rain where size sorting is significant. Two of the 2DVDs (SN37 and SN38) were deployed in mountainous terrain to determine the role of orography in DSD characteristics. These two 2DVDs were over 100 km from NPOL with radar beam height 3.2 and 2.5 km above the ground after accounting the height difference between NPOL and the two sites. Considering the greater time–height ambiguity and greater difference in sampling volumes between 2DVD and NPOL observations, the agreement in Z_H was poor at these two sites and they do not serve as a validation site for evaluating dual-polarization radar DSD retrieval algorithm.

A closer look at the NPOL-measured and 2DVD-calculated Z_H and Z_{DR} fields revealed two regimes. These regimes coincided with either under or overestimated NPOL-derived $\log(N_W)$. The combined Regimes I and II covered a considerable amount of the total observation, 9%–15%, of the coincident NPOL/2DVD database. When these regimes were removed from the database, the absolute biases were noticeably reduced for Z_H, Z_{DR}, D_{mass}, and $\log(N_W)$.

The 2DVD, a reference instrument, underestimates the concentration of small drops (Thurai and Bringi 2018)

but the addition of small drops does not correspond to either Regime I or Regime II. The implication of these nonrealistic DSD in NPOL observations could be significant for radar rainfall estimation. Hydrologists rely on radar rainfall estimates for flood forecasting and the majority of the comparative studies use rain gauges as a reference (Cunha et al. 2013). The accuracy of Z_H/Z_{DR} couples should therefore independently be evaluated prior to radar rainfall estimation. The envelope of Z_H/Z_{DR} presented here could be used a reference in these studies.

Reflectivities Z_H and Z_{DR} are vital radar measurements for radar rainfall mapping. The study presented here showed the presence of surface clutter at radar distances of less than 15 km even after labor-intensive radar quality control. The quality control had to be relaxed; otherwise true precipitation would be removed along with the clutter. The best agreement between point 2DVD and areal NPOL Z_H and Z_{DR} was mostly at the second elevation of the radar except for the farthest sites during IFloodS and OLYMPEx. These factors play an important role in radar rainfall and DSD parameter mapping, both of which are used to direct comparison with the GPM satellite estimates.

There are parallel efforts in comparing ground-based and DPR-based rainfall (Petracca et al. 2018) and DSD parameters over Italy and the United States (D'Adderio et al. 2018; Petersen et al. 2020). One significant aspect of the comparison process is the careful DPR to ground-based geometric volume matching that has been implemented in the Validation Network software. The similar measurement
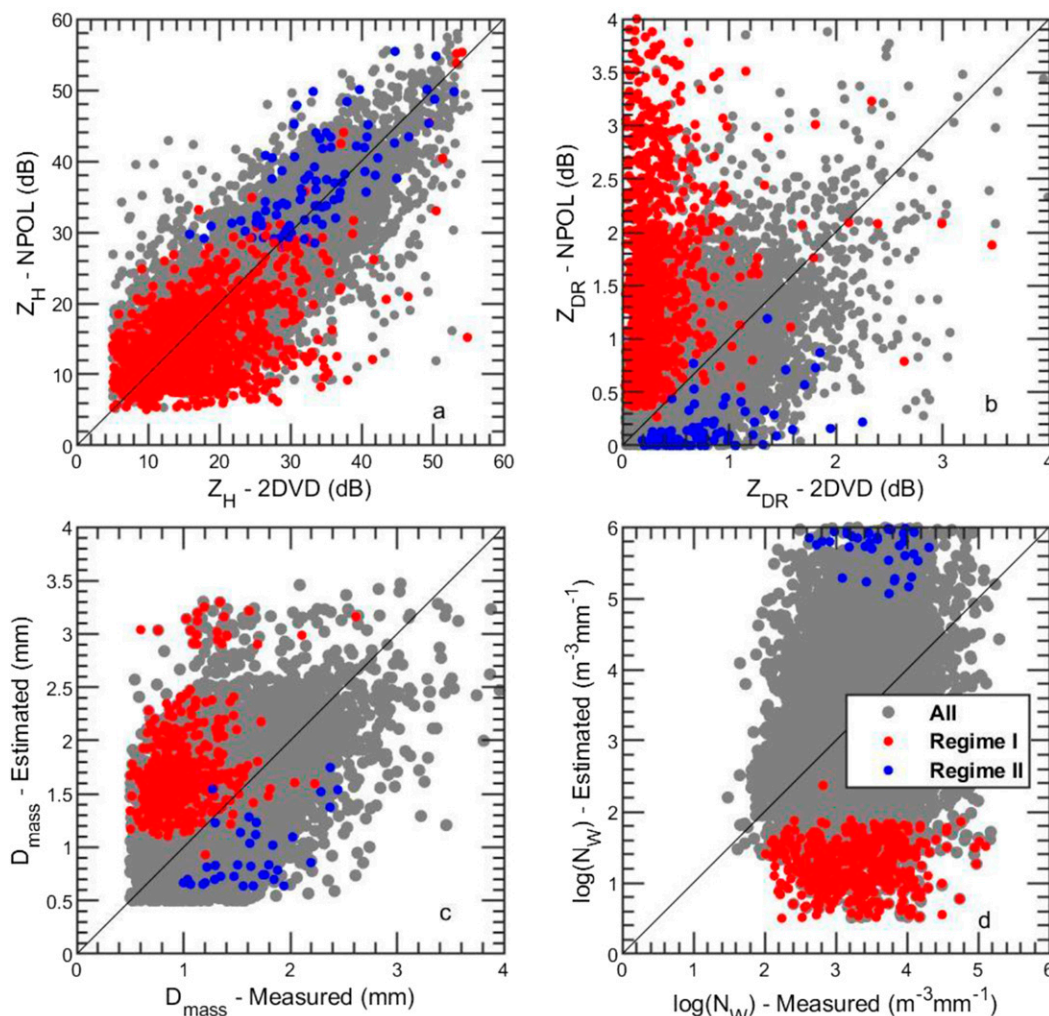
FIG. 12. Scatter diagram of 2DVD-calculated and NPOL-measured (a) Z_H and (b) Z_{DR} and 2DVD-calculated and NPOL-estimated (c) D_{mass} and (d) $\log(N_W)$. Regimes I and II were marked with red and blue circles, respectively.

type (radar) and closer spatial and temporal scales matched (Schwaller and Morris 2011) combined with an intrinsically large number of coincident samples should help to firmly establish (in a statistical sense) the degree to which the space-based estimates of the DSD converge with ground-based estimates toward demonstrating attainment of GPM level 1 science requirements that pertain to the DSD.

REFERENCES

Adirosi, E., L. Baldini, F. Lombardo, F. Russo, F. Napolitano, E. Volpi, and A. Tokay, 2015: Comparison of different fittings of drop spectra for rainfall retrievals. *Adv. Water Resour.*, **83**, 55–67, https://doi.org/10.1016/j.advwatres.2015.05.009.

Andsager, K., K. V. Beard, and N. F. Laird, 1999: Laboratory measurements of axis ratios for large raindrops. *J. Atmos. Sci.*, **56**, 2673–2683, https://doi.org/10.1175/1520-0469(1999)056<2673:LMOARF>2.0.CO;2.

Aydin, K., T. A. Seliga, and V. Balaji, 1986: Remote sensing of hail with a dual linear polarization radar. *J. Climate Appl. Meteor.*, **25**, 1475–1484, https://doi.org/10.1175/1520-0450(1986)025<1475:RSOHWA>2.0.CO;2.

Beard, K. V., and C. Chuang, 1987: A new model for the equilibrium shape of raindrops. *J. Atmos. Sci.*, **44**, 1509–1524,

https://doi.org/10.1175/1520-0469(1987)044<1509:ANMFTE>2.0.CO;2.

Brandes, E. A., G. Zhang, and J. Vivekanandan, 2004: Drop size distribution retrieval with polarimetric radar: Model an application. *J. Appl. Meteor.*, **43**, 461–475, https://doi.org/10.1175/1520-0450(2004)043<0461:DSDRWP>2.0.CO;2.

Campos, E., and I. Zawadzki, 2000: Instrumental uncertainties in Z–R relations. *J. Appl. Meteor.*, **39**, 1088–1102, https://doi.org/10.1175/1520-0450(2000)039<1088:IUIZRR>2.0.CO;2.

Cao, Q., G. Zhang, E. Brandes, T. Schuur, A. Ryzhkov, and K. Ikeda, 2008: Analysis of video disdrometer and polarimetric radar data to characterize rain microphysics in Oklahoma. *J. Appl. Meteor. Climatol.*, **47**, 2238–2255, https://doi.org/10.1175/2008JAMC1732.1.

Cifelli, R., V. Chandrasekar, S. Lim, P. C. Kennedy, Y. Wang, S. A. Rutledge, 2011: A new dual-polarization radar rainfall algorithm: Application in Colorado precipitation events. *J. Atmos. Oceanic Technol.*, **28**, 352–364, https://doi.org/10.1175/2010JTECHA1488.1.

Cunha, L. K., J. A. Smith, M. L. Baeck, and W. F. Krajewski, 2013: An early performance evaluation of the NEXRAD dual-polarization radar rainfall estimates for urban flood applications. *Wea. Forecasting*, **28**, 1478–1497, https://doi.org/10.1175/WAF-D-13-00046.1.

D'Adderio, L. P., G. Vulpiani, F. Porcu, A. Tokay, and R. Meneghini, 2018: Comparison of GPM *Core Observatory* and ground-based radar retrieval of mass-weighted mean raindrop diameter at midlatitude. *J. Hydrometeor.*, **19**, 1583–1598, https://doi.org/10.1175/JHM-D-18-0002.1.

Giangrande, S. E., and A. V. Ryzhkov, 2008: Estimation of rainfall based on the results of polarimetric echo classification. *J. Appl. Meteor. Climatol.*, **47**, 2445–2462, https://doi.org/10.1175/2008JAMC1753.1.

——, S. Collis, A. K. Theisen, and A. Tokay, 2014a: Precipitation estimation from the ARM distributed radar network during the MC3E campaign. *J. Appl. Meteor. Climatol.*, **53**, 2130–2147, https://doi.org/10.1175/JAMC-D-13-0321.1.

——, M. J. Bartholomew, M. Pope, S. Collis, and M. P. Jensen, 2014b: A summary of precipitation characteristics from the 2006-11 Northern Australian wet seasons as revealed by ARM disdrometer research facilities (Darwin, Australia). *J. Appl. Meteor. Climatol.*, **53**, 1213–1231, https://doi.org/10.1175/JAMC-D-13-0222.1.

Gorgucci, E., G. Scarchilli, and V. Chandrasekar, 1999: A procedure to calibrate multiparameter weather radar using properties of the rain medium. *IEEE Trans. Geosci. Remote Sens.*, **37**, 269–276, https://doi.org/10.1109/36.739161.

Grecu, M., W. S. Olson, S. J. Munchak, S. Ringerud, L. Liao, Z. Haddad, B. Kelley, and S. McLaughlin, 2016: The GPM combined algorithm. *J. Atmos. Oceanic Technol.*, **33**, 2225–2245, https://doi.org/10.1175/JTECH-D-16-0019.1.

Iguchi, T., S. Seto, R. Meneghini, N. Yoshida, J. Awaka, M. Le, V. Chandrasekar, and T. Kubota, 2017: GPM/DPR level-2: Algorithm theoretical basis document. GPM Doc., 68 pp., https://www.eorc.jaxa.jp/GPM/doc/algorithm/ATBD_DPR_201708_whole_1.pdf.

Kumjian, M. R., 2013: Principles and applications of dual-polarization weather radar. Part I: Description of the polarimetric radar variables. *J. Oper. Meteor.*, **1**, 226–242, https://doi.org/10.15191/nwajom.2013.0119.

Petersen, W. A., P. Kirstetter, J. Wang, D. B. Wolff, and A. Tokay, 2020: The Global Precipitation Measurement ground validation program. *Satellite Precipitation Measurement*, V. Levizzani et al., Eds., Advances in Global Change Research Series, Vol. 69, Springer-Nature, 471–502.

Petracca, M., L. P. D'Adderio, F. Porcu, G. Vulpiani, S. Sebastianelli, and S. Puca, 2018: Validation of GPM Dual-Frequency Precipitation Radar (DPR) rainfall products over Italy. *J. Hydrometeor.*, **19**, 907–925, https://doi.org/10.1175/JHM-D-17-0144.1.

Pippitt, J. L., D. B. Wolff, W. Petersen, and D. A. Marks, 2015: Data and operational processing for NASA's GPM ground validation program. *37th Conf. on Radar Meteorology*, Norman, OK, Amer. Meteor. Soc., 111, https://ams.confex.com/ams/37RADAR/webprogram/Manuscript/Paper275627/37radarmanuscript.pdf.

Ryzhkov, A. V., S. E. Giangrande, V. M. Melnikov, and T. J. Schuur, 2005: Calibration issues of dual-polarization radar measurements. *J. Atmos. Oceanic Technol.*, **22**, 1138–1155, https://doi.org/10.1175/JTECH1772.1.

Schwaller, M., and K. Morris, 2011: Ground validation network for the Global Precipitation Measurement mission. *J. Atmos. Oceanic Technol.*, **28**, 301–319, https://doi.org/10.1175/2010JTECHA1403.1.

Seto, S., T. Iguchi, and T. Oki, 2013: The basic performance of a precipitation retrieval algorithm for the Global Precipitation Measurement mission's single/dual-frequency radar measurements. *IEEE Trans. Geosci. Remote Sens.*, **51**, 5239–5251, https://doi.org/10.1109/TGRS.2012.2231686.

Silberstein, D. S., D. B. Wolff, D. A. Marks, D. Atlas, and J. L. Pippitt, 2008: Ground clutter as a monitor of radar stability at Kwajalein, RMI. *J. Atmos. Oceanic Technol.*, **25**, 2037–2045, https://doi.org/10.1175/2008JTECHA1063.1.

Skofronick-Jackson, G., and Coauthors, 2017: The Global Precipitation Measurement (GPM) mission for science and society. *Bull. Amer. Meteor. Soc.*, **98**, 1679–1695, https://doi.org/10.1175/BAMS-D-15-00306.1.

Testud, J., S. Oury, R. A. Black, P. Amayenc, and X. Dou, 2001: The concept of normalized distribution to describe raindrop spectra: A tool for cloud physics and cloud remote sensing. *J. Appl. Meteor.*, **40**, 1118–1140, https://doi.org/10.1175/1520-0450(2001)040<1118:TCONDT>2.0.CO;2.

Thompson, E. J., S. A. Rutledge, B. Dolan, and M. Thurai, 2015: Drop size distributions and radar observations of convective and stratiform rain over the equatorial Indian and west Pacific Oceans. *J. Atmos. Sci.*, **72**, 4091–4125, https://doi.org/10.1175/JAS-D-14-0206.1.

Thurai, M., and V. N. Bringi, 2018: Application of the generalized gamma model to represent the full rain drop size distribution spectra. *J. Appl. Meteor. Climatol.*, **57**, 1197–1210, https://doi.org/10.1175/JAMC-D-17-0235.1.

——, ——, L. D. Carey, P. Gatlin, E. Schultz, and W. A. Petersen, 2012: Estimating the accuracy of polarmetric radar-based retrievals of drop-size distribution parameters and rain rate: An application of error variance separation using radar-derived spatial correlations. *J. Hydrometeor.*, **13**, 1066–1079, https://doi.org/10.1175/JHM-D-11-070.1.

Tokay, A., and K. V. Beard, 1996: A field study of raindrop oscillations. Part I: Observation of size spectra and evaluation of oscillation causes. *J. Appl. Meteor.*, **35**, 1671–1687, https://doi.org/10.1175/1520-0450(1996)035<1671:AFSORO>2.0.CO;2.

——, and D. A. Short, 1996: Evidence from tropical raindrop spectra of the origin of rain from stratiform versus convective clouds. *J. Appl. Meteor.*, **35**, 355–371, https://doi.org/10.1175/1520-0450(1996)035<0355:EFTRSO>2.0.CO;2.

——, A. Kruger, W. F. Krajewski, P. A. Kucera, and A. J. Pereira Filho, 2002: Measurements of drop size distribution in the southwestern Amazon basin. *J. Geophys. Res.*, **107**, 8052, https://doi.org/10.1029/2001JD000355.

——, P. Hartmann, A. Battaglia, K. S. Gage, W. L. Clark, and C. R. Williams, 2009: A field study of reflectivity and *Z–R* relations using vertically pointing radars and disdrometers. *J. Atmos. Oceanic Technol.*, **26**, 1120–1134, https://doi.org/10.1175/2008JTECHA1163.1.

——, W. A. Petersen, P. Gatlin, and M. Wingo, 2013: Comparison of raindrop size distribution measurements by collocated disdrometers. *J. Atmos. Ocean. Technol.*, **30**, 1672–1690, https://doi.org/10.1175/JTECH-D-12-00163.1.

——, L. P. D'Adderio, D. B. Wolff, and W. A. Petersen, 2020: Development and evaluation of the raindrop size distribution parameters for the NASA Global Precipitation Measurement Mission ground validation program. *J. Atmos. Oceanic Technol.*, **37**, 115–128, https://doi.org/10.1175/JTECH-D-18-0071.1.

Ulbrich, C. W., 1983: Natural variations in the analytical form of the drop size distribution. *J. Climate Appl. Meteor.*, **22**, 1764–1775, https://doi.org/10.1175/1520-0450(1983)022<1764: NVITAF>2.0.CO;2.

Wolff, D. B., D. A. Marks, and W. A. Petersen, 2015: General application of the relative calibration adjustment (RCA) technique for monitoring and correcting radar reflectivity calibration. *J. Atmos. Oceanic Technol.*, **32**, 496–506, https://doi.org/10.1175/JTECH-D-13-00185.1.

Zagrodnik, J. P., L. A. McMurdie, and R. A. Houze Jr., 2018: Stratiform precipitation processes in cyclones passing over a coastal mountain range. *J. Atmos. Sci.*, **75**, 983–1004, https://doi.org/10.1175/JAS-D-17-0168.1.

Zeng, Y., U. Blahak, M. Neuper, and D. Jerger, 2014: Radar beam tracing methods based on atmospheric refractive index. *J. Atmos. Oceanic Technol.*, **31**, 2650–2670, https://doi.org/10.1175/JTECH-D-13-00152.1.

Zhang, G., J. Sun, and E. A. Brandes, 2006: Improving parameterization of rain microphysics with disdrometers and radar observations. *J. Atmos. Sci.*, **63**, 1273–1290, https://doi.org/10.1175/JAS3680.1.